Orientational ordering transitions of semiflexible polymers in thin films: A Monte Carlo simulation

V. A. Ivanov, A. S. Rodionova, E. A. An, J. A. Martemyanova, and M. R. Stukan*
Faculty of Physics, Moscow State University, Moscow 119991, Russia

M. Müller
Institut für Theoretische Physik, Georg-August-Universität, Friedrich-Hund-Platz 1, D-37077 Göttingen, Germany

W. Paul
Institut für Physik, Martin-Luther-Universität Halle-Wittenberg, D-06099 Halle (Saale), Germany

K. Binder
Institut für Physik, Johannes-Gutenberg-Universität, Staudinger Weg 7, D-55099 Mainz, Germany
(Received 31 May 2011; published 28 October 2011)

Athermal solutions (from dilute to concentrated) of semiflexible macromolecules confined in a film of thickness D between two hard walls are studied by means of grand-canonical lattice Monte Carlo simulation using the bond fluctuation model. This system exhibits two phase transitions as a function of the thickness of the film and polymer volume fraction. One of them is the bulk isotropic-nematic first-order transition, which ends in a critical point on decreasing the film thickness. The chemical potential at this transition decreases with decreasing film thickness ("capillary nematization"). The other transition is a continuous (or very weakly first-order) transition in the layers adjacent to the hard planar walls from the disordered phase, where the bond vectors of the macromolecules show local ordering (i.e., "preferential orientation" along the x or y axes of the simple cubic lattice, but no long-range orientational order occurs), to a quasi-two-dimensional nematic phase (with the director at each wall being oriented along either the x or y axis), while the bulk of the film is still disordered. When the chemical potential or monomer density increase, respectively, the thickness of these surface-induced nematic layers grows, causing the disappearance of the disordered region in the center of the film.

DOI: 10.1103/PhysRevE.84.041810 PACS number(s): 61.41.+e, 61.20.Ja, 64.70.M−

I. INTRODUCTION

Solutions of semiflexible polymers under good solvent conditions are known to exhibit a phase transition from an isotropic state to a nematic phase when the concentration and/or the polymer chain length sufficiently increase [1–23]. This transition is entropically driven as in standard lyotropic liquid-crystalline systems, which can be modelled as systems of hard rods or hard spherocylinders, for instance [24–26]. While for such standard liquid-crystalline systems the effect of surfaces and confinement on nematic order has already been extensively studied [27–43], the effect of walls on the orientational ordering of semiflexible macromolecules has been much less considered [44–49]. There has been a lot of work on the behavior of flexible polymers under confinement [50], but this is not our focus here. While early Monte Carlo work [44,46] mostly was concerned with investigating the local packing of the polymers near the walls, Chen *et al.* [45,48] proposed phase diagrams for the formation of nematic wetting layers at hard walls and for "capillary nematization" [32,33], analogously to "capillary condensation" [51,52] of undersaturated vapor in thin slit pores, a solution may exhibit nematic order in a capillary for conditions where it still would be isotropic in the bulk. However, the theory by Chen *et al.* [45,48] is a simple mean-field theory, inspired by Onsager's theory [24] for infinitely thin needles, based on the wormlike chain model [53–55], and, hence, neglects excluded volume effects [56].

Apart from the fact that mean-field theories in general are often inaccurate descriptions of order-disorder phenomena in particular at low dimensionality [57], for nematic systems there is an interesting complication due to the tensor character of the nematic order parameter [25]: While the order in a bulk of a nematic has uniaxial character, it is biaxial at the surface [58]. As a consequence, when in an isotropic fluid a nanoscopically thin nematic precursor layer forms near a wall (analogous to precursors of fluid wetting layers [57,59–61] of undersaturated vapor in contact with a wall), it has biaxial rather than uniaxial order. In addition, due to long wavelength fluctuations long-range nematic order in $d = 2$ dimensions should not exist, one expects an algebraic decay of orientational correlation functions and a Kosterlitz-Thouless type transition [62] to the isotropic phase [63–65]. However, the character of the nematic-isotropic transition in $d = 2$ dimensions is still not fully understood [66]. This $d = 2$ limit, however, is pertinent to our system when the bulk system is confined between two walls. Moreover, the character of the phase diagram that one expects for simple lattice models for liquid crystals confined in thin film geometry is debated. For the ordinary Lebwohl-Lasher model [67] there is evidence that the nematic-isotropic transition stays first order up to a minimum number $n_{\min}$ of lattice planes, while for $n < n_{\min}$ there is no transition whatsoever [68]. For a generalized Lebwohl-Lasher model, Fish and Vink [69] found that for some choices of parameters in the Hamiltonian there is a

*Current address: Schlumberger Dhahran Carbonate Research Center, P. O. Box 39011, Al-Khobar 31952, Saudi Arabia.

continuous transition of Kosterlitz-Thouless type for $n < n_{\min}$, down to the two-dimensional case ($n = 1$), while for other choices the transition stays first order throughout. On the basis of this evidence, they argue that the phase diagram of confined liquid-crystalline films is essentially nonuniversal.

The surface-induced ordering at the interface between a wall and a solution of semiflexible macromolecules clearly involves an interplay between the effects that the wall has on the conformations of the polymer chains [44] and the local changes in the various order parameters (local monomer density and the orientational order parameters). The situation of "complete wetting" [59–61], where a layer of nematic phase grows to macroscopic thickness on approaching phase coexistence in the semi-infinite system, is reminiscent of surface-induced ordering phenomena [70,71]. In the latter case, "critical exponents" can be introduced [70] to describe these phenomena, and it is of interest to apply this point of view to the surface-induced nematic order as well.

In the present paper, we wish to contribute toward a better understanding of these problems by grand-canonical Monte Carlo simulation of a lattice model for confined athermal solutions of semiflexible macromolecules. In previous work, the isotropic-nematic phase transition in the bulk has been carefully characterized [20,23], and the limit of extremely dilute solutions interacting with a wall (with attractive interaction between the wall and the monomeric units) has been studied [72]. The present simulations will focus on rather thick films confined by purely repulsive impenetrable flat walls, and following our work on bulk solutions of semiflexible polymers we treat a single chain length, $N = 20$. Thus, the variables of the problem are the chemical potential μ and the thickness D of the films. Thicknesses $D = 50$, 100, and 150 lattice spacings are chosen. The model and the simulation method will be briefly characterized in Sec. II, where also the quantities that will be recorded are defined. Section III describes our numerical results in detail, while Sec. IV gives a brief summary and discusses the relation to pertinent theoretical work.

II. REMARKS ON THE MODEL AND SIMULATION ASPECTS

As in our previous work on semiflexible macromolecules in bulk solution [20,23,73], we work with the bond fluctuation model [74] on the simple cubic lattice. The only interactions between the monomeric units are excluded volume interactions, while chain stiffness is controlled by an additional bending energy term, U_{bend}. Each effective monomeric unit in this model is represented by an elementary cube of the lattice. Monomer coordinates are coordinates of the front-bottom-left corner of this cube. The other seven sites at the corners of this cube are blocked from further occupation, realizing, thus, the excluded volume interaction. Taking the lattice spacing $a \equiv 1$ as the unit of length, the minimal distance between any two monomeric units is equal to 2, and the bond vectors connecting two consecutive monomeric units along the chain are taken from the set {(±2,0,0), (±2,±1,0), (±2,±1,±1), (±2,±2,±1), (±3,0,0), (±3,±1,0)}, including also all permutations between these coordinates. Altogether 108 different bond vectors occur, leading to 87 different angles between successive bonds. To describe variable chain stiffness, an intramolecular bending potential depending on the angle ϑ between two successive bond vectors along the chain is used:

$$U_{\text{bend}} = -f \cos\vartheta(1 + c\cos\vartheta), \tag{1}$$

and the parameters in Eq. (1) were chosen as $f = 8.0$ (note the convention putting $k_B T$ equal to unity) and $c = 0.03$. For this choice of parameters the isotropic to nematic transition in the bulk has already been carefully studied [23], and we need a precise knowledge about the bulk transition as a reference for our confined system. The constant c is physically insignificant and is kept here for the sake of comparison to earlier papers [13,20,23,75], while it is the parameter f that corresponds to the bending rigidity in the Kratky-Porod model [53].

Monte Carlo simulations are carried out in the grand-canonical (μVT) ensemble, which has the advantage that long-range fluctuations of the monomer density can relax rather fast. However, the difficult aspect of this ensemble in the context of Monte Carlo simulations of systems of chain molecules is the need of moves attempting to insert (or remove) a whole chain in the system, without violating the excluded volume constraint. As described in our earlier work [20,23], this difficulty is overcome by implementation of the configurational bias method [76,77]. In the configurational bias moves, one needs to utilize a biased chain insertion method to let a polymer "grow" successively into the system. At each step all possible 108 bond vectors having their origin at the current effective monomeric unit are examined, and a position for inserting the next monomeric unit along the chain is chosen, respecting the excluded volume condition, and using the Boltzmann weight calculated from the intramolecular energy, Eq. (1). The statistical weight of the generated polymer configuration hence is easily calculated recursively, and thus the bias can be accounted for in the acceptance probability for the move. In the following, one Monte Carlo step (MCS) is composed of one configurational bias move plus, additionally, either one attempt to perform a local random hopping move for all effective monomeric units in the system or one attempt of a slithering-snake move per chain.

The simulated system had the shape of a $L \times L \times D$ box, with hard impenetrable walls at $z = 0$ and $z = D + 1$, while periodic boundary conditions were used in x and y directions. As already mentioned in Sec. I, the chain length was equal to $N = 20$ monomeric units, in accord with our previous studies [20,23]. Because our potential Eq. (1) does not depend on the bond length, the equilibrium length of a free single chain totally elongated along one of the coordinate axes lies between 40 and 60. In our present simulations of confined solutions we have considered the film thicknesses $D = 50$, 100, and 150, so the smallest box width used here is of the order of a totally elongated chain. In order to check for finite-size effects, particularly in the vicinity of continuous transitions, we used several values of the linear dimension L along the walls, namely $L = 60$, 80, and 100.

In case first-order transitions are detected, the quantitative analysis of the simulations is hampered by hysteresis effects [20,23]. As explained in our earlier work [23], the most efficient recipe to cope with this problem is the application of straightforward thermodynamic integration methods. We refer to Ref. [23] for implementation details.

The chemical potential per chain μ was chosen in the range between -195 and -150 (in units of k_BT), leading to values of polymer volume fraction ϕ in the range from 0.0 up to 0.55, and it is important to distinguish between average volume fraction in the whole box and the value of the "bulk" volume fraction in the center of the box (provided a plateau is formed in the density profile in the middle of the box), which then can be compared to the "equivalent bulk density" (defined via the chemical potential and the bulk equation of state).

The total simulation time was typically between 10^7 and 2×10^7 MCS. The relaxation time in the most extreme cases (i.e., largest boxes in the vicinity of the isotropic-nematic transition) was about 5×10^6 MCS; however, this is only the nonequilibrium relaxation time in the transition region. This value characterizes the time needed for the systems to relax from a nonequilibrium state to an equilibrium one in a situation where there exist multiple states with similar free energy, especially taking into account that for the nematic phase the equilibrium state is degenerated due to multidomain structures that are discussed in more detail in subsection III B below.

We now turn to the quantities that are analyzed in the simulations. In a thin film as studied here, it is natural to calculate profiles of all collective variables (e.g., polymer volume fraction ϕ and eigenvalues S_1, S_2, S_3 of the tensor characterizing the nematic order) as a function of the z coordinate across the film, i.e., we record $\phi(z)$, $S_1(z)$, $S_2(z)$, $S_3(z)$. At this point, we recall that the tensor characterizing the nematic order is defined in terms of unit vectors $\vec{e}_i$ along the bonds connecting monomeric units i and $i+1$. In the bulk, for a system of $\mathcal{N}$ chains each having N effective monomeric units and hence $N-1$ bonds, this order-parameter tensor is

$$Q_{\alpha\beta} = \frac{1}{\mathcal{N}(N-1)} \sum_{i=1}^{\mathcal{N}(N-1)} \frac{1}{2}\left(3e_i^\alpha e_i^\beta - \delta_{\alpha\beta}\right), \qquad (2)$$

where α, β denote the Cartesian components.

The largest eigenvalue of this tensor S_1 is a good order parameter for characterizing the isotropic-nematic transition, while the combination of the second and the third eigenvalues $P = S_2 - S_3$ is known to be a good order parameter for transitions between uniaxial and biaxial phases (for a thorough discussion of the definition of order and biaxiality, see Ref. [78]). We give here a qualitative discussion of the main aspects of these order parameters only. In the bulk nematic phases all molecules show preferential alignment along one direction (the "director"), while the order of the system is rotationally invariant in the plane perpendicular to the director. Thus, in the bulk the nematic ordering is uniaxial. However, when we consider a nematic-isotropic interface, the elongated molecules align parallel to the interface: Then the direction perpendicular to the nematic director but also parallel to the interface clearly is not equivalent to the direction normal to the director and also perpendicular to the interface. Thus, in the interface (or at a hard wall) the nematic ordering has biaxial character. Of course, one should also keep in mind that in our lattice model preferred orientations of the (stretched) polymer chains and hence of the director occur along the x, y, or z axis of the simple cubic lattice only, unlike a nematic fluid in continuum space where the director can point in any direction. Likewise, when we consider surface-induced local order in a plane (or thin layer) adjacent to the wall, there are only two preferred orientations of the director, along the x axis or along the y axis. Thus, we expect that the order-disorder transition in such a layer corresponds to the Ising universality class rather than the XY class (which would possibly lead to a Kosterlitz-Thouless-type transition, as discussed in the Introduction) that applies when the director can align uniformly along any direction in the xy plane. These considerations should be kept in mind for the interpretation of our numerical results.

We have used two different averaging procedures in our simulations; we call them *averaging over profiles* and *averaging over the whole sample*. Averaging over profiles means that the average values of density, $\langle\phi\rangle$, and orientational order parameters, $\langle S_1\rangle$, $\langle S_2\rangle$, $\langle S_3\rangle$, were calculated as the mean values of their z profiles, $\phi(z)$, $S_1(z)$, $S_2(z)$, $S_3(z)$, respectively. This procedure has been used preferentially. The profiles of the orientational order parameters $S_1(z)$, $S_2(z)$, $S_3(z)$ were obtained in the following way: We calculated the orientational tensor $Q_{\alpha\beta}$ in each z layer separately, then we performed the time averaging of all these tensors $Q_{\alpha\beta}(z)$ (also separately), and at the end of the simulation run we calculated their eigenvalues. Averaging over profiles decreases the fluctuations of orientational order parameters in the isotropic phase in a system of finite size, but, on the other hand, it can lead to some artifacts when multiple nematic domains are observed in the system (such cases have been identified and corrected for possible artifacts). Averaging over the whole sample means that the average values $\bar{\phi}$, $\bar{S}_1$, $\bar{S}_2$, $\bar{S}_3$ were obtained in the course of usual time averaging of ϕ, S_1, S_2, S_3 calculated for the whole system. These quantities analyze excess properties of the confined system without referring explicitly to the internal spatial structure of the film.

In our simulations, we have recorded also standard single-chain characteristics such as the mean-square end-to-end distance R_e and the mean-square gyration radius R_g of the chains (and their components along the z axis and in the xy plane, i.e., perpendicular and parallel to the walls, as well as z profiles of all these quantities). The distribution of positions of the chain ends along the z axis has been sampled as well (cf. Ref. [79]). All these quantities depend on the polymer volume fraction $\phi = 8\mathcal{N}Na^3/V$ in the system. The average was taken over all chains and all sampled system configurations. A detailed discussion of these properties, including the interplay of chain conformations and nematic order, will be the topic of a separate publication.

III. RESULTS AND DISCUSSION

A. Profiles of the density and orientational order parameters

1. Snapshots

To help in the visualization of the different phenomena that occur in our system we start with some snapshots (Fig. 1) presenting the two-dimensional xz maps for profiles of the orientational nematic order parameter S_1. Hard walls are on the left and right side of the box, and the z axis is directed from the left to the right. In this figure we are using colors

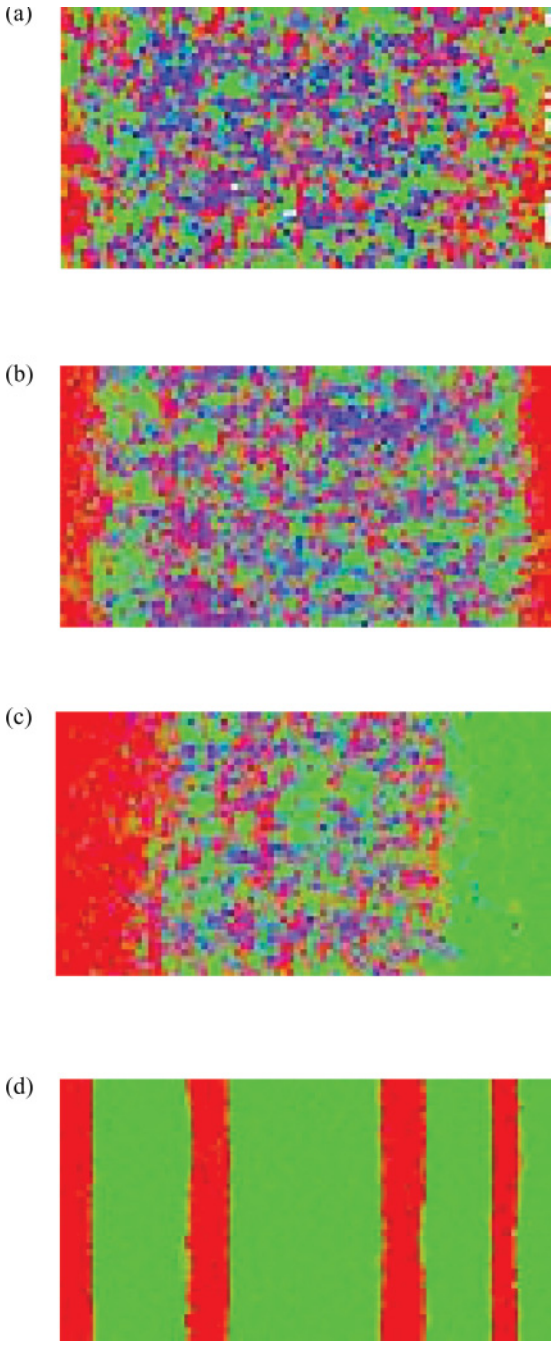

FIG. 1. (Color online) Snapshots of the simulation box of size $D = 150$ and $L_{||} = 80$ for different μ values: $\mu = -180$ (a), -171 (b), -166.4 (c), and -155 (d). The color code is explained in the text. The starting configuration was an empty box (for $\mu = -166.4$) and an isotropic solution with average volume fraction $\phi = 0.3$ (for the other three values of μ).

(grayscale) to represent the local orientation of bond vectors between monomeric units along the chain. Red (dark gray), green (light gray), and blue (middle gray) colors correspond to the orientation of bond vectors along the x, y, and z axes, respectively [80]. Green (light gray) and red (dark gray) regions indicate nematic domains oriented parallel to the walls. A blue (middle gray) region (i.e., a nematic domain with director oriented perpendicular to the walls) is never found, as expected for our model.

The profiles are shown for four different values of the chemical potential, i.e., for four different average densities (our conclusions below are based on the whole set of snapshots for all simulated values of μ, but only four of them are shown, which are typical for all possible regimes). The starting configuration was either an empty box (for $\mu = -166.4$) or an isotropic solution with average volume fraction $\phi = 0.3$ (for the other three values of μ). This means that depending on the value of the chemical potential the system can either stay isotropic if the average density (or the density in the central part of the simulation box for the case it is wide enough) lies below the isotropic-nematic transition threshold or it will jump into a nematic state after some equilibration time if the average density exceeds this threshold. Such procedure simulates the transition from isotropic to nematic state on increasing the density in the system, and we can determine the high-density boundary of the hysteresis region as the value of the chemical potential at which this jump from the isotropic into the nematic state occurs [20,23].

We observe three different regimes in Fig. 1. The first regime is $\mu \leqslant -174$ [a typical snapshot is shown for $\mu = -180$ in Fig. 1(a)], where there is no nematic ordering whatsoever in the system (neither near the walls nor in the bulk). However, some enhanced local orientation at the walls has already started—a formation of clusters of the oriented phase (nematic fluctuations) at the walls is well visible. Almost no points of perpendicular orientation (blue or middle gray) are observed at the walls. Larger domains of green (light gray) and red (dark gray) color are formed at the walls, i.e., these domains are oriented parallel to the walls (along x and y axes) but without any preferred orientation in the plane. For $\mu = -180$ the polymer volume fraction in the center of the box is around $\phi \approx 0.15$ (for comparison, the coexisting densities of the transition in the bulk [23] are $\phi_{\text{iso}} \approx 0.30$ and $\phi_{\text{nem}} \approx 0.32$, and the chemical potential at the transition is $\mu^{\text{bulk}}_{\text{trans}} \approx -166 \pm 0.5$), while there is a depletion layer at the wall where the volume fraction is around $\phi \approx 0.1$ (see Fig. 2). However, even in the limit of highly dilute solutions those chains, which have their center of mass close to the walls have to be oriented parallel to the walls.

The second regime is $-174 \leqslant \mu \leqslant -166.4$ [two typical snapshots are shown for $\mu = -171$ and $\mu = -166.4$ in Figs. 1(b) and 1(c)] where there exists pronounced nematic ordering near the walls, but the solution stays isotropic in the center of the box. In Fig. 1(b) thin domains with nematic ordering (one preferred orientation, biaxially) are formed at the walls. The two domains at both walls are both oriented along the x direction, but this occurs statistically, they could be oriented also along different directions parallel to the wall as in Fig. 1(c). In Fig. 1(c) we observe two large nematic domains at both walls, although with different orientation, and significantly less blue (middle gray) color in the center of the box, where pronounced domains parallel to x and y axes are also formed. This lack of orientation along the z axis shows that in this system bulklike behavior is no longer observed, not even in the center of the box. This system is in a state just shortly before it jumps to the nematic state, and this happens quite fast if we increase the chemical potential to the value $\mu = -166.3$. Therefore, our

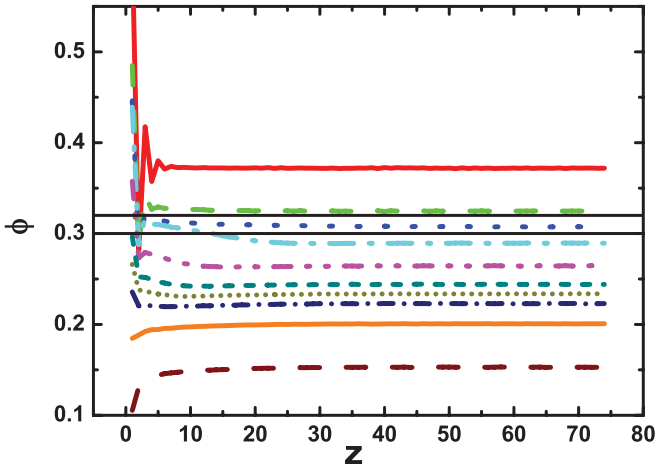

FIG. 2. (Color online) Monomer density (volume fraction) profiles for the box $D = 150$, $L = 100$ and different values of the chemical potential μ: -162, -166, -167.3, -167.4, -170, -172, -173, -174, -176, -180 (from top to bottom). Note that in this figure (and the following ones) the profiles exhibit mirror symmetry with respect to the midplane, and, hence, only the left half of the system is shown. The density values of the isotropic and nematic phases at the coexistence in the bulk are indicated by two horizontal lines. The isotropic-nematic transition in the bulk [23] takes place at $\mu_{\text{trans}}^{\text{bulk}} \approx -166$.

estimation of the high-density boundary of the isotropic-nematic transition region is $\mu = -166.4$ for this film thickness.

In the third regime, $\mu \geqslant -166.3$, the whole system is orientationally ordered and it can be either in a monodomain or in a multidomain configuration. Note that this value of the chemical potential is very close to our estimate for the nematic ordering transition in the bulk. A typical snapshot of a multidomain configuration is shown in Fig. 1(d) for the value $\mu = -155$, which is actually quite far beyond the isotropic-nematic transition point. We would like to emphasize here again that this configuration was obtained from an isotropic state after equilibration at the value of μ quoted above, i.e., without any annealing procedure by means of gradual increasing the chemical potential. Such multidomain configurations differ in their free energy only very slightly from the ground state, which is a pure, nematic monodomain configuration. Thus, in our simulation, the system is presumably kinetically trapped in a multidomain state with protracted relaxation. This problem has been already discussed in our paper on the isotropic-nematic transition in the bulk for this model [20]. We will not investigate this problem here, and we will consider both multidomain and monodomain configurations as the nematic phase. However, for a quantitative analysis of global nematic order parameters, multidomain configurations will be excluded as discussed below.

To simulate the opposite process of a transition from the nematic to the isotropic state we start with a nematic configuration of the system, e.g., a perfectly ordered dense nematic configuration, and decrease the value of the chemical potential until the system jumps into the disordered, isotropic state. This allows us to determine the low-density boundary of the hysteresis region. The results of corresponding simulation runs are discussed below.

2. *Dependence of density and orientational order-parameter profiles on the chemical potential*

Polymer density profiles (actually, polymer volume fraction profiles) and profiles of the three orientational order parameters (three eigenvalues of the orientational tensor) are shown for box size $D = 150$, $L = 100$ in Figs. 2 and 3 for different values of the chemical potential μ (indicated in the legends). We

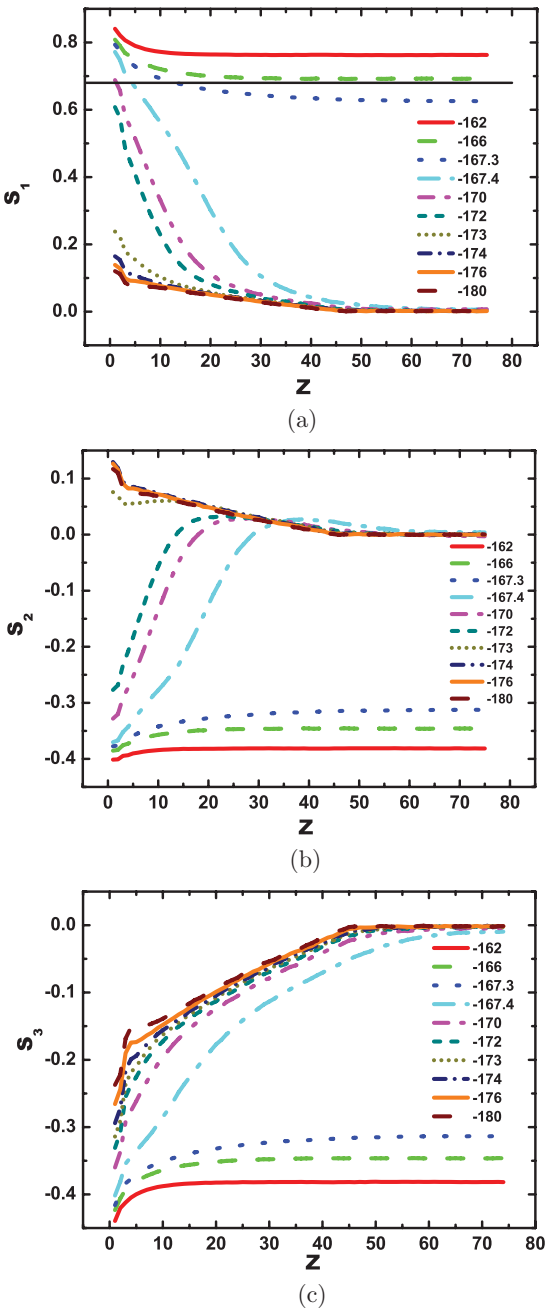

FIG. 3. (Color online) Orientational order parameter profiles $S_1(z)$ (a), $S_2(z)$ (b), $S_3(z)$ (c) for the box $D = 150$, $L = 100$ and different μ values shown in the legend. The horizontal line in the figure (a) indicates the value of the nematic order parameter at the transition in the bulk, $S_{1,\text{trans}}^{\text{bulk}} \approx 0.68$.

have verified that the profiles for the boxes of the same width $D = 150$ but with different size in the direction parallel to the walls, $L = 60$ and 80, are very similar to those presented here.

We have checked all profiles for symmetry relative to the center of the box, and we have found reasonable agreement between both parts of the profiles. All profiles have been averaged relative to the center of the box, and only one half of the box is shown in all figures displaying profiles. All profiles have been obtained in the course of an equilibration process at each particular μ value starting from a nematic monodomain configuration. This means that we can determine here actually a lower boundary of the isotropic-nematic hysteresis region.

For all average densities there is a wide plateau formed in the center of the box indicating that the box width $D = 150$ is large enough to allow for a bulk region to be formed (Fig. 2). The width of this bulk region seems to be about 100 lattice sites, although we will see below that it is actually narrower because the influence of the wall on the orientation of the polymer bonds is much more pronounced and longer ranged than the influence on the density of monomeric units. At low values of the chemical potential, $\mu \leqslant -176$, there is a depletion layer at the walls. As an analysis of the snapshots shows, in this region there nevertheless already occur nematic domains at the walls, as mentioned above. At $\mu = -176$ the polymer volume fraction in the center of the box is about $\phi_{\text{center}} \approx 0.2$. At the values of the chemical potential larger than $\mu = -174$ there is always some enhancement of polymer density at the walls. In this region $\mu \geqslant -174$, strong wall-induced orientational order occurs (see Figs. 1 and 3). Up to the value $\mu = -167.4$ a polymer layer with higher concentration has developed at both walls, and its width reaches about 20 lattice spacings at $\mu = -167.4$. Although the difference in volume fraction values between the walls and the center is not large, it is still very significant because these values lie in the vicinity of the bulk isotropic-nematic coexistence densities. Between $\mu = -167.4$ and $\mu = -167.3$ there is a well visible density jump in the center of the box to a value above the coexistence density. The densities of isotropic and nematic phases at coexistence in the bulk [23], $\phi_{\text{iso}} \approx 0.3$ and $\phi_{\text{nem}} \approx 0.32$, are indicated in Fig. 2 by two horizontal lines. One can clearly see that the densities of the isotropic and nematic phases in the center of the film just at the transition point in the whole film $\phi_{\text{iso}}^{\text{center}} \approx 0.29$ and $\phi_{\text{nem}}^{\text{center}} \approx 0.31$ lie below the corresponding densities in the bulk. On further increase of the average density, pronounced layering starts to occur at the walls.

Now let us discuss the orientational order parameter profiles in Fig. 3. First, we can see that for some μ values the width of the bulk region is not larger than about 40 lattice sites. The surface layers have larger width in comparison to the estimate based on the density profiles. There are three types of profiles for different intervals of the chemical potential. For $\mu \leqslant -173$ all three eigenvalues S_1, S_2, S_3 are very close to zero in the central part of the box, while at both walls pronounced layers of a width of about 40 lattice spacings (which is about the length of the totally elongated chain in our system) are formed where S_1 and S_2 are positive and approximately equal to each other (and their values directly at the walls are about 0.1) and S_3 is negative (about -0.2 at the wall). Such values of these parameters would correspond to an uniaxial ordering of bond vectors parallel to the walls (i.e., preferably perpendicular to the z direction). For $-172 \leqslant \mu \leqslant -167.4$ we observe several regions in the order parameter profiles: (i) a few strongly nematically ordered layers at the walls; (ii) a rather broad nematically ordered region of width about 10–15 layers; (iii) an even broader uniaxially ordered region of width about 25−30 layers [note that $S_2(z)$ is negative in region (ii) and positive in region (iii)]; (iv) an isotropic region in the center of the box. The isotropic-nematic transition in the whole film occurs at $\mu_{\text{trans}}^{(D=150)} \approx -167.3$ when the nematic order parameter in the center of the box, $S_1(z = 75)$, jumps from a very small value about 0.01 at $\mu = -167.4$ to a value of about 0.625 at $\mu = -167.3$. These values of the nematic order parameter at coexistence should be compared with those obtained for our model in the bulk, which were approximately equal to 0.01 and 0.68, respectively [23]. In the nematic film, the ordering at the walls is slightly more pronounced than that in the center of the film.

Profiles of the biaxiality order parameter $P = S_2 - S_3$ for several different values of μ for the box $D = 150$, $L = 100$ are shown in Fig. 4. We expect P to be zero inside well-developed nematic domains (and in the isotropic phase, of course) but nonzero at the location of interfaces. It is helpful to look also at the snapshots of the typical configurations shown in Fig. 1 [snapshots for $\mu = -186$ and $\mu = -174$ look quite similar to that at $\mu = -180$ shown in Fig. 1(a)]. Upon increasing μ a layer with high values of P starts to form at the wall, i.e., a surface induced quasi-two-dimensional orientational order adjacent to the walls occurs, and then the isotropic-nematic interface starts to separate (to depin) from the wall moving toward the center of the box. It disappears abruptly between $\mu = -167.4$ and -167.3 when it meets the second interface that is moving toward the center from the other wall. When "capillary nematization" occurs, the isotropic domain in the center vanishes when the two nematic-isotropic interfaces meet and annihilate each other, and then also P disappears.

Let us now turn to a discussion of finite-width effects on these transitions. The volume fraction profiles for the

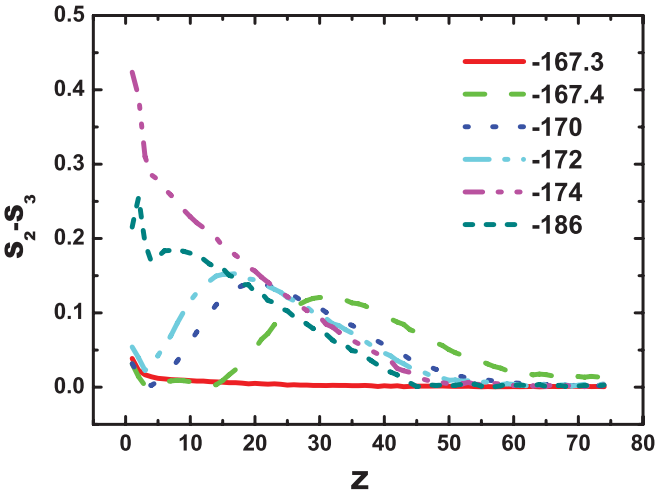

FIG. 4. (Color online) Profiles of the biaxiality parameter $P = S_2 - S_3$ for different values of μ (indicated in the legend). Simulation runs were performed in the box of sizes $D = 150$ and $L = 100$ starting from a nematic configuration. For explanation see the text.

$D = 50$ box are similar to those for $D = 150$, i.e., they show a pronounced plateau in the center of the box and first a depletion, then an increase, and, finally, some layering at the walls with increasing chemical potential (not shown). The order parameter profiles for a box of size $D = 50$ are shown in Fig. 5. This box is thin enough so the chains feel the presence of the walls in the center of the box even in a very dilute solution and stay always oriented (at least slightly) parallel to the walls. In a very dilute solution the values of the orientational order parameters in the center of the box are $S_1 \approx S_2 \approx 0.1$ and $S_3 \approx -0.2$, i.e., the system has uniaxial orientational symmetry parallel to the walls even in the center of the box (while it is increasing near the walls). With increasing the concentration of chains, we find the transition to the nematic state first at the walls and then also in the center of the box (e.g., $S_2 \approx S_3 \approx -0.4$ and $S_1 \approx 0.8$ for $\mu = -162$). Note that due to this surface-induced nematic order caused by the walls throughout the thin film we do not imply here by the use of the word *transition* that the ordering with increasing chemical potential is a (sharp) thermodynamic transition for small D. As will be discussed later, the isotropic-nematic transition in the box of width $D = 50$ occurs at $\mu_{\rm trans}^{(D=50)} \approx -169.5$ (as obtained from histogram analysis), and at this value of the chemical potential the nematic order parameter in the center of the box is about $S_1(z = 25) \approx 0.3$, while the average nematic order parameter is about $\langle S_1 \rangle \approx 0.5$ (this should be again compared to the bulk values $\mu_{\rm trans}^{\rm bulk} \approx -166$, $S_{1,\rm trans}^{\rm bulk} \approx 0.68$).

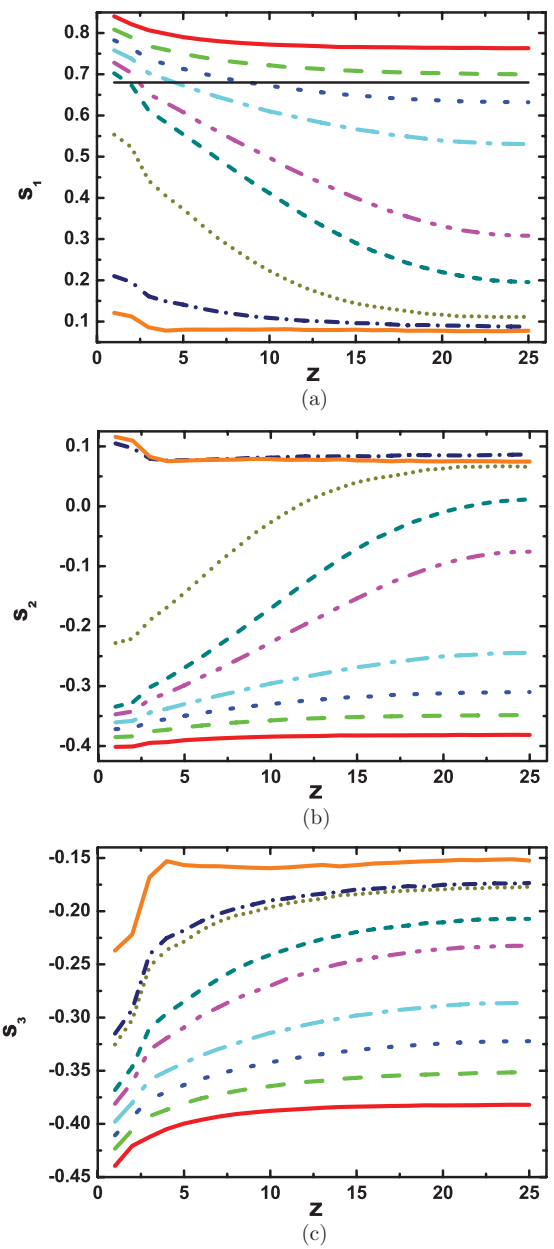

FIG. 5. (Color online) Orientational order parameter profiles $S_1(z)$ (a), $S_2(z)$ (b), $S_3(z)$ (c) for the box $D = 50$, $L = 100$ and different values of the chemical potential μ: -162, -166, -168, -169, -169.5, -170, -172.5, -173, -180 (from top to bottom in S_1 and vice versa in S_2 and S_3). The horizontal line at $S_{1,\rm trans}^{\rm bulk} \approx 0.68$ in the $S_1(z)$ plot (a) indicates the value of the nematic order parameter at the transition in the bulk.

To summarize this section, the density profiles and profiles of orientational order parameters in a film of quite large thickness show three different states (depending on the average polymer density). The first state, for $\mu < -174$ (i.e., a very dilute solution), is the isotropic phase with depletion at the walls (due to purely entropic reasons) and formation of a pronounced wide layer at the walls with preferred orientation of chains parallel to the walls but without any preferred axis in the planes parallel to the walls. The second state, for $-174 \leqslant \mu \leqslant -167.4$, is the isotropic phase with enhanced density at the walls, again, due to purely entropic reasons, and formation of a pronounced wide nematic layer at the walls with preferred orientation of chains parallel to the walls and with a preferred axis in the planes parallel to the walls. The third state, for $\mu > -167.4$, is the nematic phase with enhanced density at the walls, just after the isotropic-nematic transition took place in the whole volume of the box, and the formation of a quite narrow nematic layer at the walls (which is only a few lattice spacings thick) with larger values of the nematic order parameter. For $\mu \geqslant -162$, which we did not discuss so far, there occurs a pronounced layering at the walls extending over three to five layers in both the local volume fraction and the local nematic order parameter.

B. Dependencies of average density and average orientational order parameters on the chemical potential

We will now analyze the phase transitions underlying the above findings using the dependence of the average density and average order parameters on the chemical potential. The averaging was performed over profiles (as described in Sec. II). The dependence of the average density and orientational order parameters S_1 and $P = S_2 - S_3$ on the chemical potential μ are shown in Fig. 6 for boxes of different width $D = 50$, 100, and 150.

Simulation runs were performed at different values of the chemical potential using a monodomain nematic configuration as initial state. Two transitions are well visible in these figures. First, the nematic-isotropic transition in the center of the box occurs on decreasing the chemical potential, i.e., decreasing density, at some point around $\mu \approx -167.4$. The jump in the density is quite small, in agreement with previous studies [1,2,24]. After this transition takes place,

nematic order still exists in the film at both walls, and the average biaxiality parameter P is not equal to zero because of the presence of isotropic-nematic and nematic-wall interfaces. Then, decreasing the chemical potential further, the second transition takes place around $\mu \approx -173$, when the nematic ordering disappears completely, being exchanged by broad layers with planar orientation of bond vectors, so the biaxiality parameter P becomes even larger and then

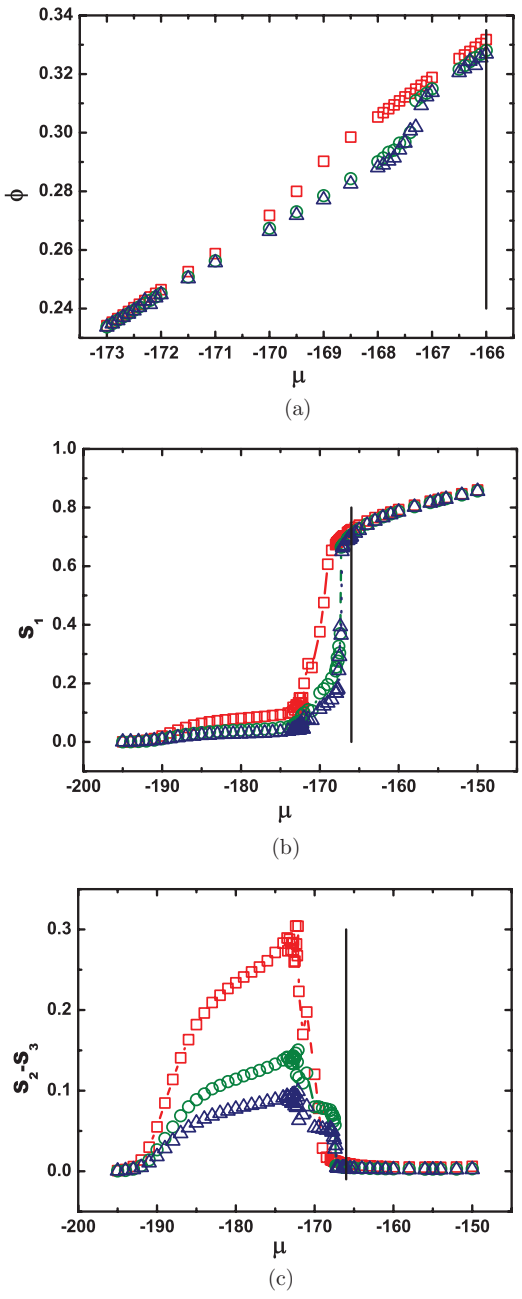

FIG. 6. (Color online) Dependencies of the average volume fraction ϕ (a), and the average orientational order parameters S_1 (b) and $P = S_2 - S_3$ (c) on the chemical potential μ for boxes of different width: $D = 50$ (red squares), $D = 100$ (green circles), and $D = 150$ (blue triangles). The box size parallel to the wall was equal to $L = 60$. The simulation runs were performed starting from a nematic configuration. The vertical line indicates the transition point in the bulk $\mu_{\text{trans}}^{\text{bulk}} = -166$.

disappears gradually on further decreasing the density down to zero. The isotropic-nematic transition is very sharp in boxes of $D = 100$ and $D = 150$ (the jumps in S_1 are quite close to each other, but a hysteresis still can be observed, see below), while it becomes smeared out in the narrow film $D = 50$ (no jumps in S_1 can be observed).

The transition where long-range orientational order at the surfaces disappears is well visible in P, slightly visible in S_1, and not visible at all in the density. This transition is also quite sharp, and it does not show any pronounced shift of the transition point as a function of the film width, although the absolute values of the biaxiality parameter P become larger with decreasing box width (since this order is merely a surface effect).

Pronounced fluctuations of S_1 and P occur in the vicinity of the surface transition [Figs. 6(b) and 6(c)]. The origin of these strong fluctuations seems to be the fact that we average here both S_1 and P over both surfaces, which order independently: Sometimes the directors of the nematic order at both walls are parallel (both oriented along the x axis or both along the y axis) and sometimes perpendicular (one along y and one along x) to each other.

In Fig. 7 we compare the average nematic order parameter and the average biaxiality order parameter as functions of the chemical potential for boxes of width $D = 150$ but of different size parallel to the walls $L = 60$, 80, and 100. We can conclude that almost no difference can be observed in those curves, so the size of the simulation box parallel to the walls is large enough to avoid systematic and significant finite-size effects.

Let us now look at a hysteresis for the average nematic order parameter $\langle S_1 \rangle$ that we observe at the isotropic-nematic phase transition for boxes $D = 100$ and $D = 150$ (Fig. 8). The comparison of runs from the nematic to the isotropic state and from the isotropic to the nematic state is presented here. For the runs from the isotropic to the nematic state the fluctuations in the nematic phase ($\mu \geqslant -166$) due to the appearance of a multidomain structure (see Fig. 9) would lead to systematically smaller values of S_1 rather than for states with a monodomain order. Since these multidomain states are easily recognizable from both snapshots as shown in Fig. 1 and from profiles (compare Figs. 3 and 9) of $S_1(z)$, we have not included these multidomain states in Fig. 8, because they would only confuse the picture and are artifacts due to the necessarily insufficient equilibration and the chosen averaging procedure. At the present moment we can define the hysteresis regions quite accurately for films of thickness $D = 100$ and 150. As regards the left (low-μ) boundary of the hysteresis region (which is observed in Fig. 8 for $N \to I$ runs), it seems that it does not depend on the film thickness for these boxes. At the same time, the right boundary of the hysteresis region (for $I \to N$ runs) does depend on the box width. The whole hysteresis region becomes smaller with decreasing film thickness, and its right boundary is displaced to lower values of μ, i.e., to lower (average) densities. For the thin film with thickness $D = 50$ the curves are rather smooth, no abrupt transition is visible, there is definitely no hysteresis, and the inflection point is shifted to lower μ clearly outside the hysteresis region for the larger D values.

Some examples of multidomain structure (which is the origin of fluctuations in the orientational order parameter in the nematic phase for the runs from isotropic initial configuration) are shown in Fig. 9. Nonsymmetrized profiles $S_1(z)$ show the

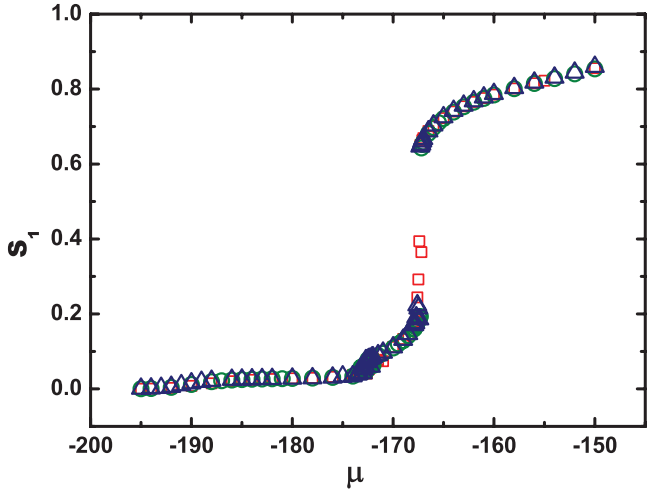

(a)

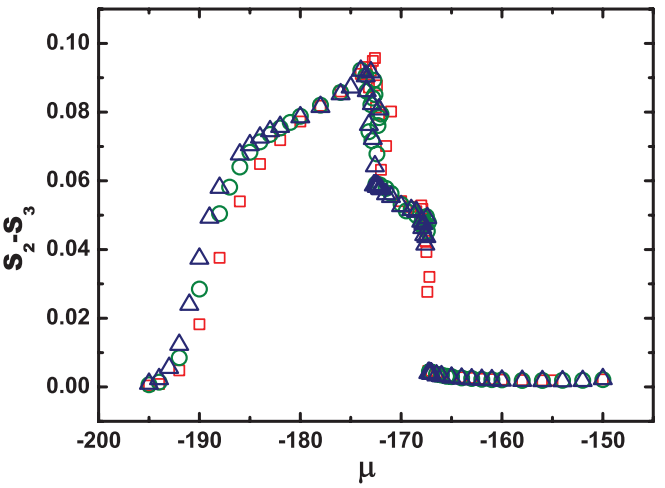

(b)

FIG. 7. (Color online) Dependencies of the average nematic order parameter S_1 (a) and biaxiality parameter $S_2 - S_3$ (b) on the chemical potential μ for boxes of different size parallel to the wall: $L = 60$ (red squares), $L = 80$ (green circles), and $L = 100$ (blue triangles). The box width was equal to $D = 150$. The simulation runs were performed starting from a nematic configuration.

presence of several domains separated by interfaces at which S_1 has much lower values. These configurations were obtained from an initially isotropic solution at different μ values. For $\mu = -161$, which is not far away from the transition point, the interface is broader, while for $\mu = -150$ the interfaces are very narrow. We would like to emphasize here that these profiles demonstrate the system behavior averaged over time, in contrast to snapshots in Fig. 1 that show only an instantaneous picture. These profiles were our tool to determine multidomain structures and to eliminate them from our sampling.

In Fig. 10 we present the dependencies of the polymer volume fraction and nematic order parameter on the chemical potential for the box $D = 150$, $L = 100$. We compare here the dependencies of the average values $\langle\phi\rangle$ and $\langle S_1\rangle$ (averaged over the spatial variation) and those of the plateau values ϕ^{plateau} and S_1^{plateau} (calculated by averaging over the plateau in the corresponding profiles in the central part of the film). For the film of thickness $D = 150$ the width of the plateau in the center of the box was about 30–40 layers for $S_1(z)$ profiles and about 90–100 layers for $\phi(z)$ profiles. The data for simulation runs starting both from a nematic and from an isotropic configuration are presented, and the presence of a hysteresis is observed. Those data points in S_1 that are due to multidomain configurations have been identified and are not included here. This hysteresis can be compared with that observed in the bulk: The bulk data from our previous simulations [20] are denoted by large open rhombs and squares and the bulk transition point $\mu_{\text{trans}}^{\text{bulk}} = -166$ is denoted by a vertical solid line. Plateau values ϕ^{plateau} and S_1^{plateau} lie systematically below the average values $\langle\phi\rangle$ and $\langle S_1\rangle$ and almost coincide with the corresponding bulk values.

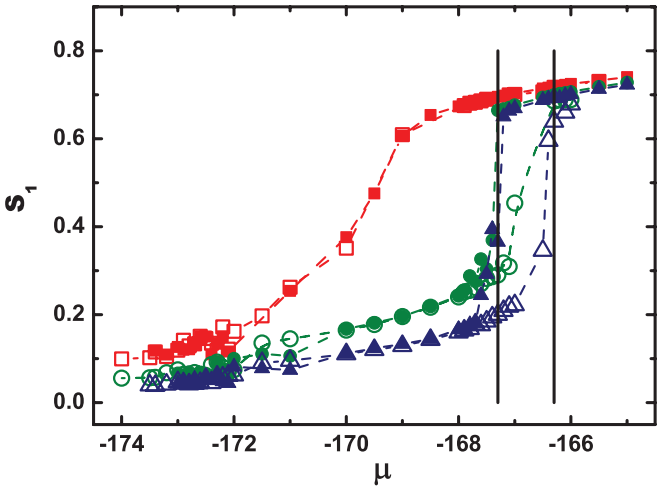

FIG. 8. (Color online) The average nematic order parameter $\langle S_1\rangle$ plotted versus the chemical potential μ for boxes of different width: $D = 50$ (red squares), $D = 100$ (green circles), and $D = 150$ (blue triangles). The box size parallel to the wall was equal to $L = 60$. A comparison of runs from the nematic to the isotropic state (full symbols) and from the isotropic to the nematic state (open symbols) is presented. The hysteresis region for the box of width $D = 150$ (at $\mu_{\text{left}} = -167.3$ and $\mu_{\text{right}} = -166.3$) is marked by two vertical lines.

The values of the chemical potential for the left, $\mu_{\text{left}} \approx -167.3$, and the right, $\mu_{\text{right}} \approx -166.3$, boundaries of the hysteresis region for the box of size $D = 150$, $L = 100$ (Fig. 10) obtained from the data both for S_1^{plateau} and $\langle S_1\rangle$ coincide very well with those obtained from the average $\langle S_1\rangle$ for the box of size $D = 150$, $L = 60$ (Fig. 8). A very narrow hysteresis is also visible for S_1^{plateau} and $\langle S_1\rangle$ for the box of width $D = 100$ (data are not shown): $\mu_{\text{left}} \approx -167.3$, $\mu_{\text{right}} \approx -167.0$. For $D = 50$ we observe no hysteresis either for $\langle S_1\rangle$ or for S_1^{center} (the value of the nematic order parameter at the center of the box). The left and right boundaries of the hysteresis in the bulk (not shown here) were $\mu \approx -167.5$ and $\mu \approx -164$, respectively [20]. Therefore, we can conclude that the left boundaries of the hysteresis both in $\langle S_1\rangle$ and S_1^{plateau} coincide well with each other and with the bulk value, while the right boundary is shifted to lower values of the average density on decreasing the film width. Consequently, the width of the hysteresis region becomes narrower on decreasing the film thickness, and the middle point of the hysteresis region is also shifted to lower values of the average density.

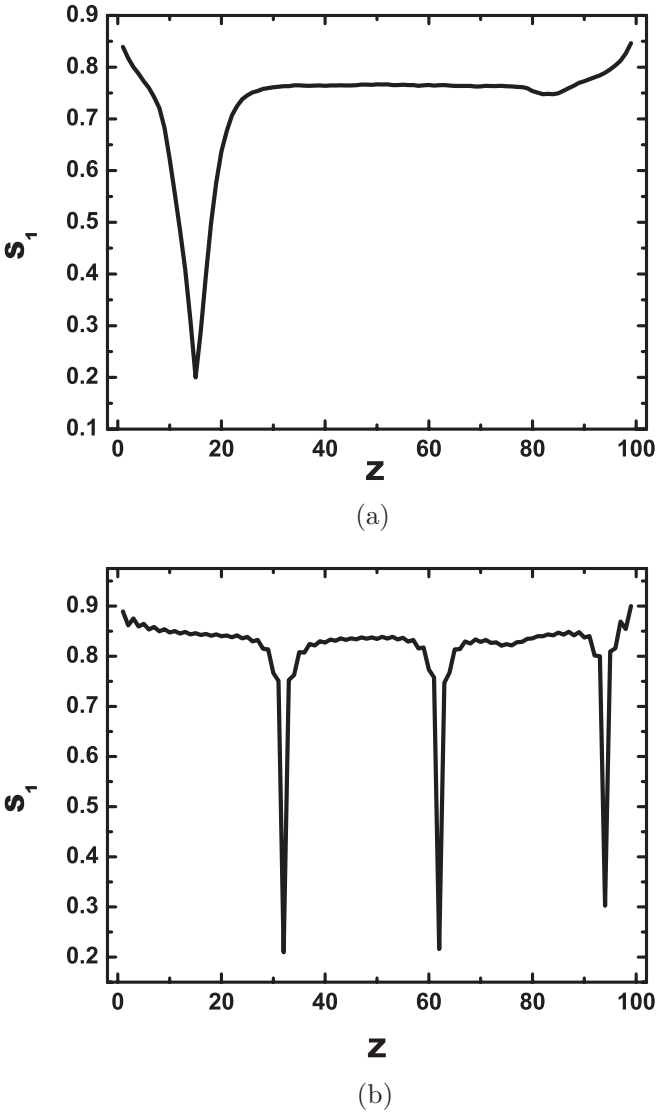

FIG. 9. Profiles of the nematic order parameter S_1 for values of the chemical potential $\mu = -161$ (a) and -150 (b), where a multidomain structure appears, and for box of size $D = 100$ and $L = 60$. Isotropic starting configurations were used for all these runs. Nonsymmetrized profiles are shown here.

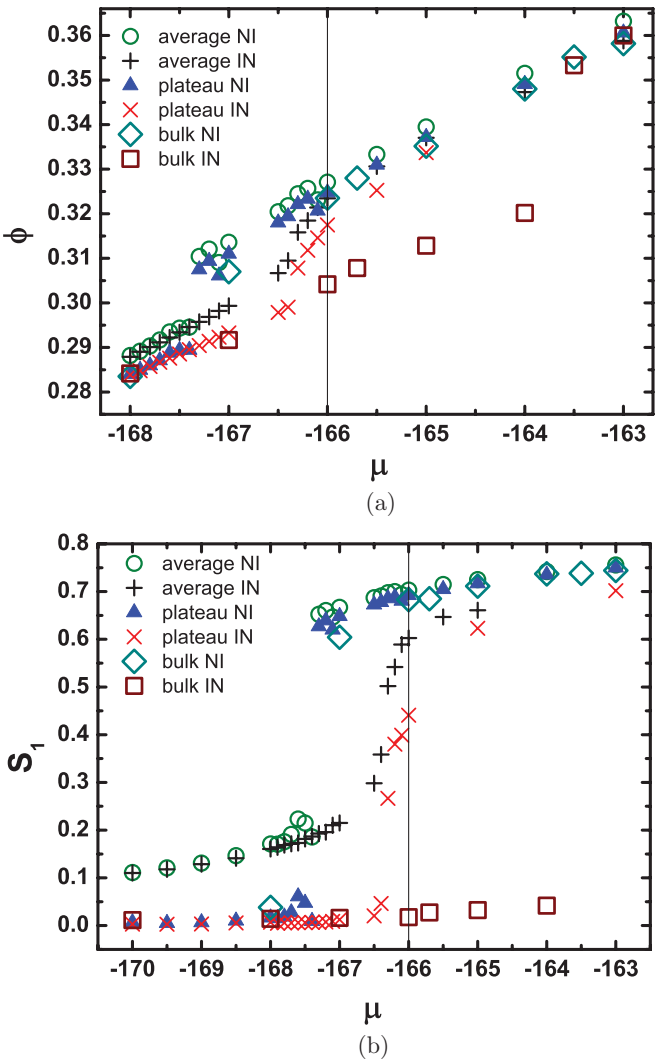

FIG. 10. (Color online) The average volume fraction and its plateau value in the center of the box (a) and the average nematic order parameter S_1 and its plateau value in the center of the box (b) plotted versus the chemical potential μ. All data for the confined solutions are for box sizes $D = 150$ and $L = 100$. Bulk data from previous simulations [20] are added as well. A comparison of runs from the nematic to the isotropic state and from the isotropic to the nematic state is presented. Symbols for different values are explained in the legend. The vertical line indicates the nematic transition in the bulk $\mu_{\text{trans}}^{\text{bulk}} = -166$.

We expect that the bulk behavior will be observed for the plateau values ϕ^{plateau} and S_1^{plateau} if the box width is large enough. However, it is not obvious whether the bulk behavior is re-established in the center of the slit even when there is a well defined (but narrow) plateau. It seems that for our system the film of $D = 150$ is not thick enough to render the profiles starting at the left wall and the right wall strictly noninteracting in the center of the film, i.e., in the film $D = 150$ the bulk behavior is not yet precisely reproduced in the central part of the box, because we observe a shift of the hysteresis in the μ dependencies of the plateau values S_1^{plateau} in comparison to the true bulk.

The capillary nematization, i.e., the shift of the isotropic-nematic transition point $\Delta\mu = \mu_{\text{trans}}^{\text{bulk}} - \mu_{\text{trans}}(D)$ in the film of finite thickness D, can be quantified using the dependencies of the average nematic order parameter $\langle S_1 \rangle$ on the chemical potential μ and taking the middle point of the hysteresis region as an estimate of the transition point $\mu_{\text{trans}}(D)$. One would expect that the data for μ_{trans} exhibit a $1/D$ correction.

C. On the order of the observed transitions

While it is clear from the discussed data, that the isotropic-nematic transition in the bulk of the film is a first-order transition for $D = 100$ and $D = 150$, it is not obvious from Figs. 5, 6, and 8 whether the transition for $D = 50$ is still first order or already continuous. Furthermore, it is not obvious what the order of surface-ordering transition is. As discussed, this should be a continuous transition in a continuum model,

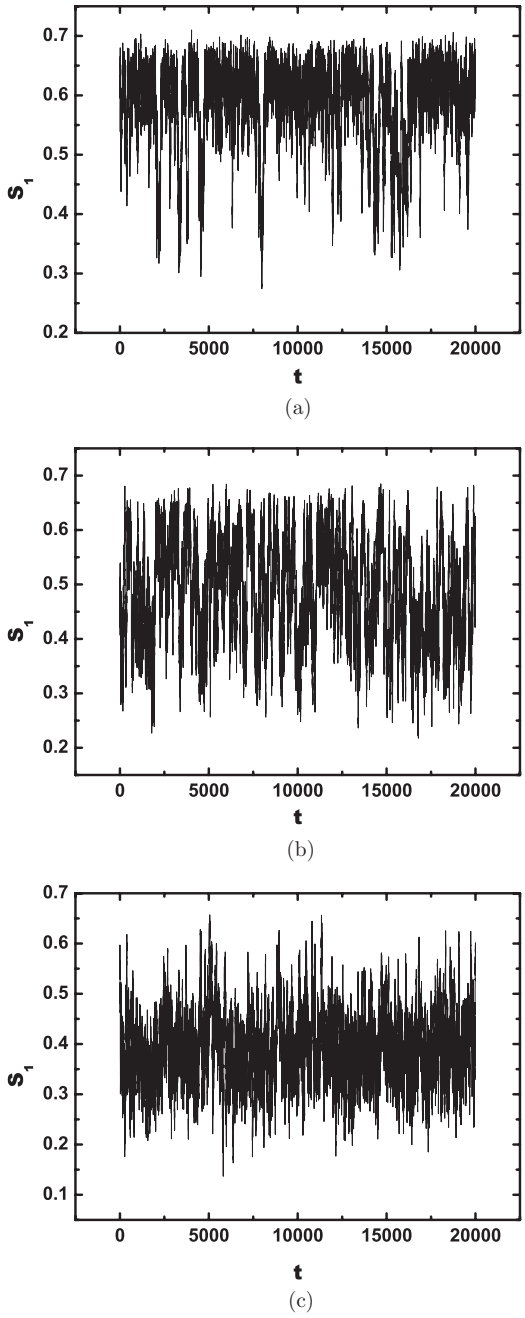

FIG. 11. Time series for the orientational order parameter S_1 for the box $D = 50$, $L = 60$ at $\mu = -169.1$ (a), -169.5 (b), -169.9 (c) close to the isotropic-nematic transition in a rather thin film.

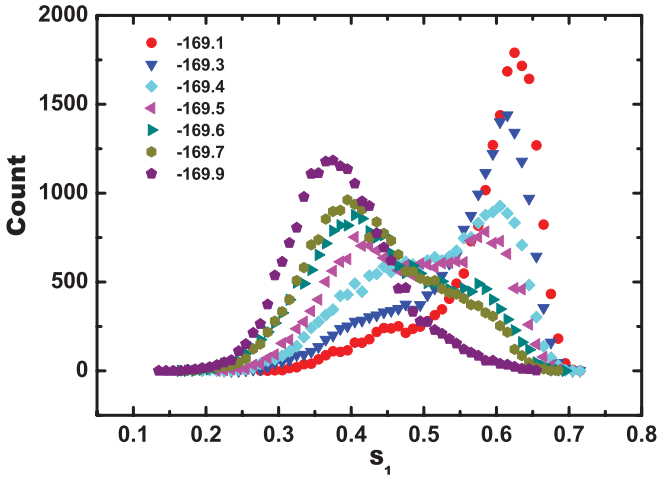

FIG. 12. (Color online) Non-normalized histograms of the nematic orientational order parameter S_1 for the box $D = 50$, $L = 60$ and for values of the chemical potential $-170 < \mu < -169$.

but we are studying a lattice model with an *a priori* broken rotation invariance parallel to the walls.

To have a closer look at the order of the bulk transition for $D = 50$ we are displaying in Figs. 11 and 12 time series and probability distributions for the largest eigenvalue, S_1, of the Saupe tensor for the whole simulation box. In Fig. 11 we are showing time series of S_1 in the nematic phase close to the transition, $\mu = -169.1$ [Fig. 11(a)], at the transition, $\mu = -169.5$ [Fig. 11(b)], and in the isotropic phase, $\mu = -169.9$ [Fig. 11(c)]. These time series demonstrate the quality of the sampling and multiple switches between coexisting states around $S_1 \simeq 0.4$ and 0.6 during the simulation run. The coexistence between the isotropic phase ($S_1 \simeq 0.38$) and the nematic phase ($S_1 \simeq 0.62$) in Fig. 11(b) is better visible when we look at the corresponding histograms for the occurrence of specific values of S_1 in these time series that are displayed in Fig. 12. The bimodality of the distribution and the shift of weight between the isotropic and the nematic phase as a function of chemical potential can be clearly observed. From the comparison with the simulation results obtained for liquid crystal models in confinement [32,33] we would expect to see a critical endpoint for the line of first-order phase transitions in the bulk at a distance between the walls that is roughly equal to the linear size of the molecules. The character of the transition in a thin film in the off-lattice model and the bond fluctuation model, however, differs markedly as discussed in the Introduction. In our case, we can take the observed value for the end-to-end distance of the chains as a measure for the size of the molecules. For our chains it is $R_e \approx 25$, so $D = 50$ is on the order of $2R_e$. From this argument we would expect the transition to be only weakly first order at best, as we seem to observe here.

An assessment of the order of the surface transition can be only tentative on the basis of our data. When we look at the biaxiality parameter P displayed in Figs. 6(c) and 7(b) there seem to occur two jumps as a function of chemical potential. The one at the larger value of μ is due to the bulk ordering. The one at lower value $\mu \simeq -173$ does not depend on D in its location but only in its relative magnitude compared to the bulk transition. The biaxiality parameter is sensitive to the presence of isotropic-nematic interfaces and nematic-wall interfaces in the system. Unfortunately, the values we can obtain in the transition region around $\mu = -173$ are rather noisy, so a closer inspection of the curves in Figs. 6 and 7 gives no conclusive evidence on the character of the transition. When we look at the histograms of P obtained from time series similar to those of Fig. 11 we cannot observe a clear indication of bimodality; see Fig. 13 (we show in this figure the data for the box of width $D = 50$ because the surface transition is better visible in this case, and we have calculated the biaxiality parameter in the left half of the box to avoid artifacts due to different

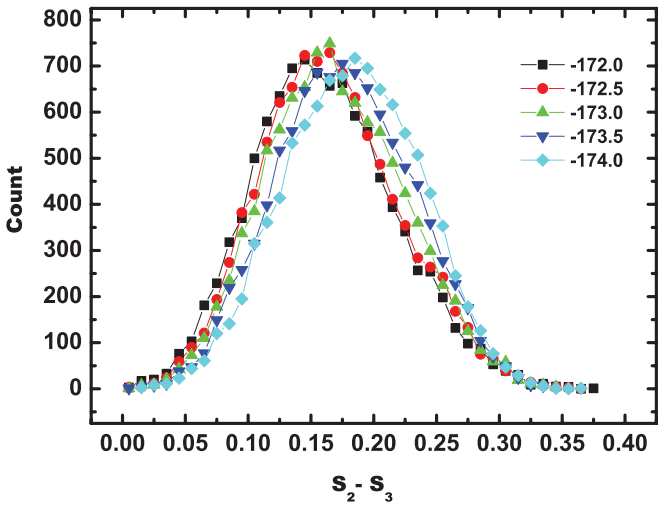

FIG. 13. (Color online) Non-normalized histograms of $S_2 - S_3$ calculated from time series of S_2 and S_3 accumulated in the left half of the box. The box size was equal to $D = 50$, $L = 60$. The runs were performed starting from the nematic state.

orientation of the nematic director at both walls). However, the distributions are rather broad and asymmetric, so we cannot rule out that they are due to two strong overlapping peaks that are only slightly separated. In conclusion, our data are at this stage compatible with a continuous or very weakly first-order transition at the surfaces of our system.

D. Phase diagram

The phase diagram in the variables inverse thickness of the film, $1/D$, vs. the chemical potential, μ, shows two transitions (Fig. 14). One of them is the isotropic-nematic first-order transition that supposedly ends up in a critical point on decreasing the film thickness. The isotropic-nematic transition points for the boxes of differing width D were

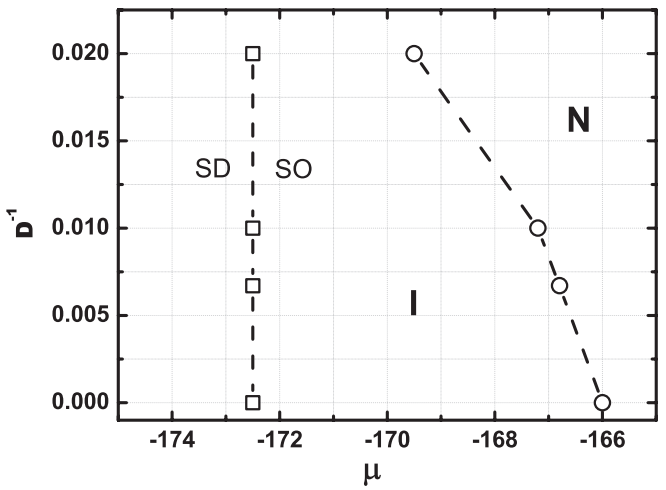

FIG. 14. Phase diagram in the variables inverse film width, $1/D$, vs. chemical potential, μ. **N** denotes the region of stability of the nematic phase, and **I** denotes the region of stability of the isotropic phase where the surfaces can be either disordered (SD, "surface disordered") or nematically ordered (SO, "surface ordered").

obtained as the middle points of the hysteresis regions on the dependencies of S_1 on μ for each particular box width. The other transition is the surface-induced orientational transition from an essentially disordered phase (at the smallest chemical potentials or monomer densities, respectively) to a phase where near both walls orientational long-range order occurs, the director being aligned either along the x direction or the y direction of the square lattice, respectively, while the bulk of the film remains still disordered. For thick enough films, the ordering at both walls occurs essentially independently of each other, and, thus, it may happen that at one wall alignment along the x axis and at the other wall alignment along the y axis occurs (cf. Fig. 1). Note that hard walls disfavor alignment along the z direction, and, thus, small nonzero values of the biaxiality order parameter P are already found in the orientationally disordered phase right near the wall (Fig. 4). The surface transition is characterized by a rapid rise of both S_1 and P in the first few lattice places adjacent to the wall (Figs. 3 and 4). When one studies P as function of μ averaging P over the whole film, the surface transition is marked by a maximum of P (Figs. 6 and 7). This transition shows up in the vicinity of both walls and its correlation length perpendicular to a wall is about the gyration radius of a single chain. A caveat should be added here regarding the fact that in our system the "surface disordered" (SD) state corresponds to the uniaxial (U) ordering at the walls in the continuum model of hard rods [32,33], while the "surface ordered" (SO) state corresponds to the biaxial ordering at the walls in that model.

IV. CONCLUSIONS AND OUTLOOK

In the present work, we have considered the effect of confinement on an athermal solution of semiflexible polymers that can undergo a transition from an isotropic phase to a nematic phase when the monomer density increases. This isotropic-nematic transition in the bulk has been studied in our earlier work, by large-scale Monte Carlo simulation of a lattice model, which allows for orientation of the nematic director along the x, y, or z axes of the lattice, respectively. The chosen Hamiltonian would, in principle, allow an orientation of the director along nontrivial directions on the lattice, but, due to entropic reasons, orientations along the lattice directions are preferred. The confinement of such a system between two parallel hard walls, a distance D along the z axis apart, strongly favors the orientation of the polymers (which behave almost like rigid rods in the ordered phase) along the x or y axes, while an orientation of the nematic director in z direction is strongly suppressed. Thus, hard walls act like "fields" coupling to the nematic order parameter, favoring the orientation of the director parallel to the wall but disfavoring the orientation perpendicular to it.

On a qualitative level, one can expect that this model will show an overall tendency of wall-induced nematic order, leading in thin films to an order-disorder transition that occurs, then, at smaller monomer densities than in the bulk: i.e., "capillary nematization" occurs. Of course, due to the anisotropy of the lattice our model fails to exhibit the rotation symmetry around the z axis that a solution of semiflexible polymers in the continuum space confined by two parallel hard walls would exhibit.

We find that in our model this transition from the disordered solution toward nematic order occurs in two steps: For rather dilute solutions, the system is disordered everywhere. When we examine the orientations of individual bond vectors, we find that only in the immediate vicinity of the walls bond vectors with a z component are strongly suppressed, but apart from this bias due to the walls, bond vector orientations are almost uncorrelated. However, when the density of monomers (or the chemical potential μ) increases, larger orientationally ordered clusters appear, localized near the walls. This enhancement of local order continues until, at $\mu \approx -173$, a continuous (or very weakly first-order) transition to two-dimensional long-range order in a thin layer adjacent to the walls occurs. The situation is similar to complete wetting in the vicinity of the prewetting critical point, where, on approaching the bulk transition, the preferred (ordered) phase exhibits a rapid variation of its thickness. Note that for large D the two surface layers are not correlated with each other, and since the directors in both layers can be either parallel (both oriented along the x axis or both oriented along the y axis) or perpendicular to each other (one director oriented along the x axis and the other along the y axis) the correct analysis of the total order parameters S_1 and $P = S_2 - S_3$ in the system is subtle. Note that (when the total thin film develops a monodomain nematic order) only S_1 is nonzero for $D \to \infty$, but for finite D when the system is still disordered in the bulk but nematically ordered near the walls, P is nonzero in the nematic-isotropic interfacial regions, and, thus, a nonzero biaxiality order parameter exists in thin films over a broad regime of monomer densities (or μ) as an interfacial effect (Fig. 6). Figure 4 shows very clearly that $P(z)$ is largest near the wall, when the nematic-isotropic interface is "tightly bound" to the wall, close to the transition of the surface from a disordered to an orientationally ordered state. When the chemical potential and monomer density increase, the thickness of the nematically ordered surface layers grows, the nematic-isotropic interface "unbinds" from the wall, and $P(z)$ now has its maximum inside the film, not near the wall. The interfaces propagate from the walls toward the interior of the film and start to interact for the film thickness considered in the simulations. Eventually, the whole system can make its transition to the uniformly ordered nematic phase, and $P(z)$ is very close to zero everywhere. Our results hence confirm the interpretation of "capillary nematization" as a consequence of a surface-induced ordering, where first a two-dimensional transition toward an ordered surface layer occurs, which then grows in thickness as the transition in the bulk is approached, consistent with the general description as an "interface unbinding" similar to the approach toward complete wetting at vapor-to-liquid transitions. Unlike the latter, of course, the surface does not uniquely favor one particular value of the "order parameter," and, thus, in our model a (Ising-type) two-dimensional (in the sense of the dimension of the order parameter) phase transition (breaking the symmetry between orientational order parallel to the x axis or the y axis) necessarily must precede the formation of a nematic layer (that otherwise is analogous to the "wetting-like" layer in the vapor-to-liquid transition case). Thus, it is plausible that this "surface transition" (from the disordered to the nematically ordered state of the surface) occurs at a chemical potential that is independent of film thickness, D, while the transition where nematic order spreads out in the whole film ("capillary nematization") strongly depends on D (and ends at a minimal value of D, where the two ordered layers formed at the surface transition interact immediately, leaving no space for a well-developed disordered phase in the center of the film and, hence, causing an immediate but gradual nematic ordering of such an ultrathin film).

It would be very interesting to look for the phenomena as described above in experiments on real systems. Gratifyingly, a nematic surface transition has very recently been observed, in a thermally driven system at a temperature where the bulk still is isotropic [81]. This work reports the surface transition to be clearly of first order, unlike our second-order or only weakly first-order transition, but the difference may be due to thermotropic effects that are completely absent in our simulation. Of course, in real systems the director can, furthermore, align in any direction parallel to the surface plane; it is not restricted to the two lattice directions as in our model. Thus, the issue of a possible Kosterlitz-Thouless transition is not relevant for our model, while it may be relevant for real systems. Moreover, the polymeric aspect, which is very important in our model, is outside the scope of consideration here. The subject of interplay between chain conformations and nematic order will be treated in another paper. It would be also interesting to vary the chain stiffness and to study its influence on the properties of these systems, e.g., smaller stiffness may give rise to an interesting interplay between width of the ordered surface layer and the chain extension, and we plan to consider this point in our next publications. We do hope, however, that our model system studies will nevertheless stimulate more experimental work on this fascinating topic of surface-induced liquid-crystalline order.

ACKNOWLEDGMENTS

We acknowledge the financial support from DFG and RFBR (joint project Grants 436 RUS 113/791 and 09-03-91339). Very useful discussions with A. Semenov, F. Schmid, T. Schilling, and A. Emelyanenko are kindly appreciated. Simulations were performed on the supercomputer SKIF at MSU. V. I. also acknowledges financial support from the Russian Ministry of Education and Science (Contract No. 16.523.12.3001).

[1] P. J. Flory, Proc. R. Soc. London A **234**, 60 (1956); **234**, 73 (1956).

[2] A. R. Khokhlov and A. N. Semenov, Physica A **108**, 546 (1981); **112**, 605 (1982); A. N. Semenov and A. R. Khokhlov, Sov. Phys. Usp. **31**, 988 (1988).

[3] T. Odijk, Macromolecules **19**, 2313 (1986).

[4] A. Baumgärtner, J. Chem. Phys. **84**, 1905 (1986).

[5] A. Kolinski, J. Skolnick, and R. Yaris, Macromolecules **19**, 2560 (1986).

[6] *Liquid Crystallinity in Polymers: Principles and Fundamental Properties*, edited by A. Ciferri (VCH, New York, 1991).

[7] M. R. Wilson and M. P. Allen, Mol. Phys. **80**, 277 (1993).

[8] S. Fraden, G. Maret, and D. L. D. Caspar, Phys. Rev. E **48**, 2816 (1993); J. Tang and S. Fraden, Liq. Cryst. **19**, 459 (1995).

[9] M. Dijkstra and D. Frenkel, Phys. Rev. E **51**, 5891 (1995).

[10] W.-L. Chen, T. Sato, and A. Teramoto, Macromolecules **31**, 6506 (1998).

[11] K. Kassapidou, W. Jesse, J. A. P. P. van Dijk, and J. R. C. van der Maarel, Biopolymers **46**, 31 (1998).

[12] A. Yethiraj and H. Fynewever, Molec. Phys. **93**, 693 (1998); H. Fynewever and A. Yethiraj, J. Chem. Phys. **108**, 1636 (1998).

[13] H. Weber, W. Paul, and K. Binder, Phys. Rev. E **59**, 2168 (1999).

[14] G. T. Pickett and K. S. Schweizer, J. Chem. Phys. **110**, 6597 (1999).

[15] H. H. Strey, V. A. Parsegian, and R. Podgornik, Phys. Rev. E **59**, 999 (1999).

[16] K. M. Jaffer, S. B. Opps, D. E. Sullivan, B. G. Nickel, and L. Mederos, J. Chem. Phys. **114**, 3314 (2001).

[17] Y. Dong, Y. Wu, J. Wang, and M. Wang, Eur. Polym. J. **37**, 1713 (2001).

[18] C. Vega, C. McBride, and L. G. MacDowell, J. Chem. Phys. **115**, 4203 (2001); C. McBride, C. Vega, and L. G. MacDowell, Phys. Rev. E **64**, 011703 (2001); C. Vega, C. McBride, and L. G. MacDowell, PhysChemChemPhys **4**, 853 (2002); C. McBride and C. Vega, J. Chem. Phys. **117**, 10370 (2002).

[19] P. P. F. Wessels and B. M. Mulder, Soft Materials **1**, 313 (2003).

[20] V. A. Ivanov, M. R. Stukan, M. Müller, W. Paul, and K. Binder, J. Chem. Phys. **118**, 10333 (2003).

[21] K. R. Purdy and S. Fraden, Phys. Rev. E **70**, 061703 (2004).

[22] X. J. Lü and J. T. Kindt, J. Chem. Phys. **120**, 10328 (2004).

[23] V. A. Ivanov, E. A. An, L. A. Spirin, M. R. Stukan, M. Müller, W. Paul, and K. Binder, Phys. Rev. E **76**, 026702 (2007).

[24] L. Onsager, Ann. NY Acad. Sci. **51**, 627 (1949).

[25] P. G. de Gennes and J. Prost, *The Physics of Liquid Crystals*, 2nd ed. (Clarendon, Oxford, 1992).

[26] G. J. Vroege and H. N. W. Lekkerkerker, Rep. Prog. Phys. **55**, 1241 (1992).

[27] P. Sheng, Phys. Rev. Lett. **37**, 1059 (1976); Phys. Rev. A **26**, 1610 (1982).

[28] T. J. Sluckin and A. Poniewierski, Phys. Rev. Lett. **55**, 2907 (1985); A. Poniewierski and T. J. Sluckin, Liq. Cryst. **2**, 281 (1987).

[29] T. J. Sluckin and A. Poniewierski, in *Fluid Interfacial Phenomena*, edited by C. A. Croxton, Chap. 5 (Wiley, New York, 1986) p. 215.

[30] A. Poniewierski, Phys. Rev. E **47**, 3396 (1993).

[31] I. Rodriguez-Ponce, J. M. Romero-Enrique, E. Velasco, L. Mederos, and L. F. Rull, Phys. Rev. Lett. **82**, 2697 (1999); J. Phys. Condens. Matter **12**, A363 (2000).

[32] R. van Roij, M. Dijkstra, and R. Evans, Europhys. Lett. **49**, 350 (2000).

[33] M. Dijkstra, R. van Roij, and R. Evans, Phys. Rev. E **63**, 051703 (2001).

[34] A. Chrzanowska, P. I. C. Teixeira, H. Ehrentraut, and D. J. Cleaver, J. Phys. Condens. Matter **13**, 4715 (2001).

[35] I. Rodriguez-Ponce, J. M. Romero-Enrique, and L. F. Rull, Phys. Rev. E **64**, 051704 (2001).

[36] L. Harnau and S. Dietrich, Phys. Rev. E **66**, 051702 (2002).

[37] H. Steuer, S. Hess, and M. Schoen, Phys. Rev. E **69**, 031708 (2004).

[38] D. de las Heras, E. Velasco, and L. Mederos, J. Chem. Phys. **120**, 4949 (2004).

[39] K. Shundyak and R. van Roij, Europhys. Lett. **74**, 1039 (2006).

[40] H. Reich and M. Schmidt, J. Phys. Condens. Matter **19**, 326103 (2007).

[41] Y. Martinez-Raton, Phys. Rev. E **75**, 051708 (2007).

[42] A. J. McDonald, M. P. Allen, and F. Schmid, Phys. Rev. E **63**, 010701(R) (2000); N. Akino, F. Schmid, and M. P. Allen, *ibid.* **63**, 041706 (2001).

[43] R. L. C. Vink, S. Wolfsheimer, and T. Schilling, J. Chem. Phys. **123**, 074901 (2005).

[44] A. Yethiraj, J. Chem. Phys. **101**, 2489 (1994).

[45] Z. Y. Chen and S.-M. Cui, Phys. Rev. E **52**, 3876 (1995).

[46] F. A. Escobedo and J. J. de Pablo, J. Chem. Phys. **106**, 9858 (1997).

[47] D. Micheletti, L. Muccioli, R. Berardi, M. Ricci, and C. Zannoni, J. Chem. Phys. **123**, 224705 (2005).

[48] J. Z. Y. Chen, D. E. Sullivan, and X. Yuan, Europhys. Lett. **72**, 89 (2005); Macromolecules **40**, 1187 (2007).

[49] P. Cifra and I. Teraoka, Macromolecules **36**, 9638 (2003); Z. Skrinarova and P. Cifra, Macromol. Theory Simul. **11**, 401 (2002); **10**, 523 (2001).

[50] M. Alcoutlabi and G. B. McKenna, J. Phys. Condens. Matter **17**, R461 (2005); J. Baschnagel and F. Varnik, *ibid.* **17**, R851 (2005); K. Binder, Annu. Rev. Mater. Res. **38**, 123 (2008); J.-L. Barrat, J. Baschnagel, and A. Lyulin, Soft Matter **6**, 3430 (2010); R. von Klitzing, E. Thormann, T. Nylander, D. Langevin, and C. Stubenrauch, Adv. Colloid Interface Sci. **155**, 19 (2010).

[51] R. Evans, J. Phys. Condens. Matter **2**, 8989 (1990).

[52] L. D. Gelb, K. E. Gubbins, R. Radhakrishnan, and M. Sliwinska-Bartkowiak, Rep. Prog. Phys. **62**, 1573 (1999).

[53] O. Kratky and G. Porod, Rec. Trav. Chim. Pays-Bas. **68**, 1106 (1949).

[54] K. F. Freed, Adv. Chem. Phys. **22**, 1 (1972).

[55] J. Des Cloizeaux and G. Jannink, *Polymers in Solution: Their Modelling and Structure* (Oxford University Press, 1990).

[56] H.-P. Hsu, W. Paul, and K. Binder, Europhys. Lett. **92**, 28003 (2010).

[57] K. Binder, in *Cohesion and Structure of Surfaces*, edited by D. G. Pettifor (Elsevier Science, Amsterdam, 1995), p. 121.

[58] Z. Y. Chen, Phys. Rev. E **47**, 3765 (1993).

[59] D. E. Sullivan and M. M. Telo da Gama, in *Fluid Interfacial Phenomena*, edited by C. A. Croxton (Wiley, New York, 1986), p. 45.

[60] S. Dietrich, in *Phase Transitions and Critical Phenomena*, edited by C. Domb and J. Lebowitz, Vol. XII (Academic Press, New York, 1988), p. 1.

[61] K. Binder, D. P. Landau, and M. Müller, J. Stat. Phys. **110**, 1411 (2003).

[62] J. M. Kosterlitz and D. J. Thouless, J. Phys. C: Solid State Phys. **6**, 1181 (1973).

[63] M. Dijkstra and D. Frenkel, Phys. Rev. E **50**, 349 (1994).

[64] M. A. Bates and D. Frenkel, J. Chem. Phys. **112**, 10034 (2000).

[65] M. C. Lagomarsino, M. Dogterom, and M. Dijkstra, J. Chem. Phys. **119**, 3535 (2003).

[66] R. L. C. Vink, Phys. Rev. Lett. **98**, 217801 (2007); H. H. Wensink and R. L. C. Vink, J. Phys. Condens. Matter **19**, 466109 (2007); J. M. Fish and R. L. C. Vink, Phys. Rev. B **80**, 014107 (2009).

[67] P. A. Lebwohl and G. Lasher, Phys. Rev. A **6**, 426 (1972).

[68] R. Paredes, A. I. Fariñas-Sánchez, and R. Botet, Phys. Rev. E **78**, 051706 (2008); A. I. Fariñas-Sánchez, R. Botet, B. Berche, and R. Paredes, Condens. Matter Phys. **13**, 13601 (2010); e-print arXiv:0906.4079v1.

[69] J. M. Fish and R. L. C. Vink, Phys. Rev. E **81**, 021705 (2010).

[70] R. Lipowsky, Phys. Rev. Lett. **49**, 1575 (1982); Z. Phys. B **51**, 165 (1983); J. Appl. Phys. **55**, 2485 (1984).

[71] W. Schweika, K. Binder, and D. P. Landau, Phys. Rev. Lett. **65**, 3321 (1990); W. Schweika, D. P. Landau, and K. Binder, Phys. Rev. B **53**, 8937 (1996).

[72] V. A. Ivanov and J. A. Martemyanova, Macromol. Symp. **252**, 12 (2007); V. A. Ivanov, J. A. Martemyanova, M. Müller, W. Paul, and K. Binder, J. Phys. Chem. B **113**, 3653 (2009).

[73] M. R. Stukan, V. A. Ivanov, M. Müller, W. Paul, and K. Binder, ePolymers, no. 062 (2003).

[74] I. Carmesin and K. Kremer, Macromolecules **21**, 2819 (1988); H.-P. Deutsch and K. Binder, J. Chem. Phys. **94**, 2294 (1991).

[75] Historically the parameter c in the bending potential came from a mapping procedure of a realistic polymer model onto the bond-fluctuation lattice model [W. Paul and N. Pistoor, Macromolecules **27**, 1249 (1994)].

[76] D. Frenkel and B. Smit, *Undestanding Molecular Simulation: From Algorithms to Applications*, 2nd ed. (Academic Press, San Diego, 2002).

[77] J. I. Siepmann, Mol. Phys. **70**, 1145 (1990); G. C. A. M. Mooij and D. Frenkel, *ibid*. **74**, 41 (1991); J. I. Siepmann and D. Frenkel, *ibid*. **75**, 59 (1992); D. Frenkel and B. Smit, *ibid*. **75**, 983 (1992).

[78] R. J. Low, Eur. J. Phys. **23**, 111 (2002).

[79] J.-S. Wang and K. Binder, J. Phys. I (France) **1**, 1583 (1991).

[80] More precisely, the red, R, green, G, and blue, B, components of the RGB set of the color of a point with coordinates (x,z) are calculated as the normalized sum of those bond vectors which have the origin at the same (x,z) coordinates (further details of the calculation method can be found in Ref. [73]).

[81] S. Aya, Yu. Sasaki, F. Araoka, K. Ema, K. Ishikawa, A. V. Emelyanenko, and H. Takezoe, Phys. Rev. Lett. **106**, 117801 (2011).